AIAA JOURNAL
Vol. 40, No. 5, May 2002

Computation of Unsteady Nonlinear Flows in Cascades Using a Harmonic Balance Technique

Kenneth C. Hall,* Jeffrey P. Thomas,† and W. S. Clark‡
Duke University, Durham, North Carolina 27708-0300

A harmonic balance technique for modeling unsteady nonlinear flows in turbomachinery is presented. The analysis exploits the fact that many unsteady flows of interest in turbomachinery are periodic in time. Thus, the unsteady flow conservation variables may be represented by a Fourier series in time with spatially varying coefficients. This assumption leads to a harmonic balance form of the Euler or Navier–Stokes equations, which, in turn, can be solved efficiently as a steady problem using conventional computational fluid dynamic (CFD) methods, including pseudotime time marching with local time stepping and multigrid acceleration. Thus, the method is computationally efficient, at least one to two orders of magnitude faster than conventional nonlinear time-domain CFD simulations. Computational results for unsteady, transonic, viscous flow in the front stage rotor of a high-pressure compressor demonstrate that even strongly nonlinear flows can be modeled to engineering accuracy with a small number of terms retained in the Fourier series representation of the flow. Furthermore, in some cases, fluid nonlinearities are found to be important for surprisingly small blade vibrations.

Introduction

UNTIL recently, most aerodynamic analyses of unsteady flows in turbomachinery blade rows have been one of two types: nonlinear time-domain analyses or time-linearized frequency-domain analyses. In the time-domain approach (see, for example, Refs. 1–6), one discretizes the fluid equations of motion on a computational grid. The flow solution is then marched from one time level to the next using conventional computational fluid dynamic (CFD) techniques, subject to appropriate unsteady boundary conditions, for example, arising from the prescribed motion of the airfoil. The advantages of this approach are that it is relatively straightforward to implement and can model nonlinear as well as linear disturbances. However, because of the need for such schemes to be both time accurate and stable, the size of the time step will generally be quite small, especially for explicit schemes, leading to excessively large computational times.

Using the frequency-domain or time-linearized technique (see, for example, Refs. 7–13), one first computes the time-mean (steady) flow by solving the steady flow equations using conventional CFD techniques. One then assumes that any unsteadiness in the flow is small and harmonic in time ($e^{j\omega t}$). The governing fluid equations of motion and the associated boundary conditions are then linearized about the mean flow solution to arrive at a set of linear variable coefficient equations that describe the small disturbance flow. The time derivatives $\partial/\partial t$ are replaced by $j\omega$, where ω is the frequency of the unsteady disturbance, so that time does not appear explicitly. The resulting time-linearized equations can be solved very inexpensively, but unfortunately cannot model dynamic nonlinearities.

In this paper, a novel harmonic balance technique for computing unsteady nonlinear flows in turbomachinery cascades is presented. The unsteady flow is represented by a Fourier series in time with frequencies that are integer multiples of the fundamental excitation frequency, blade passing frequency in the case of wake/rotor interaction, or the blade vibratory frequency in the case of flutter. We then use a harmonic balance technique to write a set of coupled partial differential equations for the unknown Fourier coefficients of the flowfield. A pseudotime term is introduced into the harmonic balance equations so that the equations can be solved using conventional time-marching CFD techniques. The present harmonic balance method has some similarities to the SLiQ approach proposed by Giles[14] and the harmonic analysis approach proposed by He and Ning[15] and Ning and He[16] but is more general than either of the latter two methods.

Governing Equations

In strong conservation law form, the two-dimensional Reynolds-averaged Navier–Stokes equations are given by

$$\frac{\mathrm{d}}{\mathrm{d}t}\int\int_D \boldsymbol{U}\,\mathrm{d}x\,\mathrm{d}y + \oint_{\partial D}\left(\boldsymbol{F} - \boldsymbol{U}\frac{\partial f}{\partial t}\right)\mathrm{d}y - \oint_{\partial D}\left(\boldsymbol{G} - \boldsymbol{U}\frac{\partial g}{\partial t}\right)\mathrm{d}x = \int\int_D \boldsymbol{S}\,\mathrm{d}x\,\mathrm{d}y \tag{1}$$

where D is a deforming control volume bounded by the control surface ∂D. The quantities $\partial f/\partial t$ and $\partial g/\partial t$ are the x and y components of the velocity of the control surface ∂D. The vector of conservation variables $\boldsymbol{U}$, the flux vectors $\boldsymbol{F}$ and $\boldsymbol{G}$, and the source term vector $\boldsymbol{S}$ are given by

$$\boldsymbol{U} = \begin{bmatrix} \rho \\ \rho u \\ \rho v \\ \rho e \\ \rho\tilde{\nu} \end{bmatrix}, \qquad \boldsymbol{F} = \begin{bmatrix} \rho u \\ \rho u^2 + p - \tau_{xx} \\ \rho uv - \tau_{xy} \\ \rho uh - \tau_{hx} \\ \rho u\tilde{\nu} - \tau_{\nu x} \end{bmatrix}$$

$$\boldsymbol{G} = \begin{bmatrix} \rho v \\ \rho uv - \tau_{xy} \\ \rho v^2 + p - \tau_{yy} \\ \rho vh - \tau_{hy} \\ \rho v\tilde{\nu} - \tau_{\nu y} \end{bmatrix}, \qquad \boldsymbol{S} = \begin{bmatrix} 0 \\ 0 \\ 0 \\ 0 \\ S_t \end{bmatrix} \tag{2}$$

The first four equations are the conservation of mass, axial and circumferential momentum, and energy, respectively. In the preceding equations, ρ is the density; u and v are the velocity components in the x and y directions, respectively; e is the total internal energy; h is the total enthalpy; and p is the static pressure. For an ideal gas with

Received 1 February 2001; revision received 15 October 2001; accepted for publication 31 October 2001.

*Professor and Chair, Department of Mechanical Engineering and Materials Science. Associate Fellow AIAA.
†Research Assistant Professor, Department of Mechanical Engineering and Materials Science. Member AIAA.
‡Research Assistant Professor, Department of Mechanical Engineering and Materials Science; currently Manager of Turbomachinery Aerodynamics, Analysis and Design Application Company, Ltd., Plymouth, MI 48170.

constant specific heats, the pressure and enthalpy may be expressed in terms of the conservation variables, that is,

$$h = (\rho e + p)/\rho \tag{3}$$

$$p = (\gamma - 1)\{\rho e - (1/2\rho)[(\rho u)^2 + (\rho v)^2]\} \tag{4}$$

The shear stresses τ_{xx}, τ_{xy}, and τ_{yy} are given by

$$\tau_{xx} = (\mu + \mu_t)\left(\frac{4}{3}\frac{\partial u}{\partial x} - \frac{2}{3}\frac{\partial v}{\partial y}\right) \tag{5}$$

$$\tau_{xy} = (\mu + \mu_t)\left(\frac{\partial u}{\partial y} + \frac{\partial v}{\partial x}\right) \tag{6}$$

$$\tau_{yy} = (\mu + \mu_t)\left(\frac{4}{3}\frac{\partial v}{\partial y} - \frac{2}{3}\frac{\partial u}{\partial x}\right) \tag{7}$$

where μ, μ_t, and ν are the molecular viscosity, the turbulent viscosity, and the kinematic viscosity, respectively. The terms τ_{hx} and τ_{hy} in the energy equation are given by

$$\tau_{hx} = u\tau_{xx} + v\tau_{xy} - q_x \tag{8}$$

$$\tau_{hy} = u\tau_{xy} + v\tau_{yy} - q_y \tag{9}$$

where q_x and q_y are the x and y components of the heat flux, respectively, and can be written as

$$q_x = -\left(\frac{\mu c_p}{Pr} + \frac{\mu_t c_p}{Pr_t}\right)\frac{\partial T}{\partial x} \tag{10}$$

$$q_y = -\left(\frac{\mu c_p}{Pr} + \frac{\mu_t c_p}{Pr_t}\right)\frac{\partial T}{\partial y} \tag{11}$$

where c_p is the specific heat at constant pressure, T is the temperature, and Pr and Pr_t are the laminar and turbulent Prandtl numbers, respectively.

In the present study, the laminar coefficient of viscosity is determined from Sutherland's law. The turbulent viscosity is modeled using the one-equation turbulence model due to Spalart and Allmaras[17]; the fifth equation in Eqs. (1) and (2) is the Spalart–Allmaras turbulence model written in strong conservation form. It describes the convection, production, and destruction of the turbulent viscosity μ_t in terms of $\tilde{\nu}$, the working conservation variable. In the present study, the flow is assumed to be fully turbulent, that is, no transition model is used.

Harmonic Balance Analysis

To motivate the development of the harmonic balance analysis, and for simplicity, we assume for the moment that the flow in a blade row is two dimensional, inviscid, and nonheat conducting, with constant specific heats. Thus, the flow may be modeled by the two-dimensional Euler equations, that is,

$$\frac{\partial \boldsymbol{U}}{\partial t} + \frac{\partial \boldsymbol{F}(\boldsymbol{U})}{\partial x} + \frac{\partial \boldsymbol{G}(\boldsymbol{U})}{\partial y} = 0 \tag{12}$$

where now the vector of conservation variables $\boldsymbol{U}$ and the flux vectors $\boldsymbol{F}$ and $\boldsymbol{G}$ are given by

$$\boldsymbol{U} = \begin{Bmatrix} \rho \\ \rho u \\ \rho v \\ \rho e \end{Bmatrix}, \qquad \boldsymbol{F} = \begin{Bmatrix} \rho u \\ \rho u^2 + p \\ \rho uv \\ \rho uh \end{Bmatrix}, \qquad \boldsymbol{G} = \begin{Bmatrix} \rho v \\ \rho uv \\ \rho v^2 + p \\ \rho vh \end{Bmatrix} \tag{13}$$

In this paper, we consider unsteady flows that are temporally and spatially periodic. In particular, temporal periodicity requires that

$$\boldsymbol{U}(x, y, t) = \boldsymbol{U}(x, y, t + T) \tag{14}$$

where T is the temporal period of the unsteadiness. Similarly, for cascade flow problems arising from vibration of the airfoils with fixed interblade phase angles σ, or incident gusts that are spatially periodic, spatial periodicity requires that

$$\boldsymbol{U}(x, y + G, t) = \boldsymbol{U}(x, y, t + \Delta T) \tag{15}$$

where G is the blade-to-blade gap and ΔT is the time lag associated with the interblade phase lag. As an example, consider a cascade of airfoils where the source of aerodynamic excitation is blade vibration with a prescribed interblade phase angle σ and frequency ω. Then $T = 2\pi/\omega$ and $\Delta T = \sigma/\omega$.

Because the flow is temporally periodic, the flow variables may be represented as a Fourier series in time with spatially varying coefficients. For example, the conservation variables may be expressed as

$$\begin{aligned} \rho(x, y, t) &= \sum_n R_n(x, y)e^{j\omega nt} \\ \rho u(x, y, t) &= \sum_n U_n(x, y)e^{j\omega nt} \\ \rho v(x, y, t) &= \sum_n V_n(x, y)e^{j\omega nt} \\ \rho e(x, y, t) &= \sum_n E_n(x, y)e^{j\omega nt} \end{aligned} \tag{16}$$

where, in principle, the summations are taken over all integer values of n. In practice, these series are truncated to a finite number of terms, $-N \le n \le +N$. Note that, in Eqs. (3), (4), and (13), the only conservation variable to appear in the denominator of any term is ρ. To motivate the development of one possible form of the harmonic balance analysis, it will be convenient to represent $1/\rho$ in a Fourier series. Therefore, we let

$$\frac{1}{\rho(x, y, t)} = \sum_n \Gamma_n(x, y)e^{j\omega nt} \tag{17}$$

To determine the coefficients Γ_n in terms of the coefficients R_n, we require that

$$\rho \cdot \frac{1}{\rho} = \left[\sum_n R_n(x, y)e^{j\omega nt}\right] \times \left[\sum_m \Gamma_m(x, y)e^{j\omega mt}\right] = 1 \tag{18}$$

We require all of the terms in the resulting Fourier series be zero, except the zero-frequency terms, that is, $m + n = 0$, which should sum to unity. If R_n is known, then using this harmonic balance, one can solve a linear system of equations for Γ_m. For example, suppose that in our harmonic balance analysis we retain frequencies up to twice the fundamental forcing frequency ω. Then the solution to Eq. (18) is given approximately by

$$\begin{bmatrix} R_0 & R_{-1} & R_{-2} & & \\ R_1 & R_0 & R_{-1} & R_{-2} & \\ R_2 & R_1 & R_0 & R_{-1} & R_{-2} \\ & R_2 & R_1 & R_0 & R_{-1} \\ & & R_2 & R_1 & R_0 \end{bmatrix} \begin{Bmatrix} \Gamma_{-2} \\ \Gamma_{-1} \\ \Gamma_0 \\ \Gamma_1 \\ \Gamma_2 \end{Bmatrix} = \begin{Bmatrix} 0 \\ 0 \\ 1 \\ 0 \\ 0 \end{Bmatrix} \tag{19}$$

This result is approximate because the product of the two truncated Fourier series produces a Fourier series with frequencies up to twice those in the original series. With the harmonic balance technique, Eq. (18) is only satisfied up to the highest frequency in the original series.

Next, we substitute the series expansions for $1/\rho$, ρ, ρu, ρv, and ρe into the Euler equations. For example, the conservation of axial momentum is given by

$$\sum_m j\omega m U_m(x, y)\exp(j\omega m t) + \frac{\partial}{\partial x}\left\{(\gamma-1)\sum_m E_m \exp(j\omega m t) - \frac{\gamma-3}{2}\sum_m\sum_n\sum_l \Gamma_m(x, y)U_n(x, y)U_l(x, y)\exp[j\omega(m + n + l)t] - \frac{\gamma-1}{2}\sum_m\sum_n\sum_l \Gamma_m(x, y)V_n(x, y)V_l(x, y) \times \exp[j\omega(m+n+l)t]\right\} + \frac{\partial}{\partial y}\left\{\sum_m\sum_n\sum_l \Gamma_m(x, y) \times U_n(x, y)V_l(x, y)\exp[j\omega(m+n+l)t]\right\} = 0 \tag{20}$$

Similar expressions can be derived for the conservation of mass and energy.

Next, we group the terms in Eq. (20) by frequency and require each frequency component to satisfy Eq. (20) individually, at least for each frequency in the original series. Collecting the resulting equations together, including the equivalent mass and energy equations, into one vector equation gives

$$\frac{\partial \tilde{\boldsymbol{F}}(\tilde{\boldsymbol{U}})}{\partial x} + \frac{\partial \tilde{\boldsymbol{G}}(\tilde{\boldsymbol{U}})}{\partial y} + \tilde{\boldsymbol{S}}(\tilde{\boldsymbol{U}}) = 0 \tag{21}$$

where

$$\tilde{\boldsymbol{U}} = \begin{Bmatrix} R_0 \\ U_0 \\ V_0 \\ E_0 \\ R_{+1} \\ U_{+1} \\ V_{+1} \\ E_{+1} \\ \vdots \end{Bmatrix}, \qquad \tilde{\boldsymbol{S}} = j\omega \begin{Bmatrix} 0\cdot R_0 \\ 0\cdot U_0 \\ 0\cdot V_0 \\ 0\cdot E_0 \\ +1\cdot R_{+1} \\ +1\cdot U_{+1} \\ +1\cdot V_{+1} \\ +1\cdot E_{+1} \\ \vdots \end{Bmatrix} \tag{22}$$

$$\tilde{\boldsymbol{F}} = \begin{Bmatrix} U_0 \\ (\gamma-1)E_0 - \frac{\gamma-3}{2}\sum \Gamma_m U_n U_{0-m-n} - \frac{\gamma-1}{2}\sum \Gamma_m V_n V_{0-m-n} \\ \gamma\sum \Gamma_m U_n E_{0-m-n} - \frac{\gamma-1}{2}\sum \Gamma_m\Gamma_n U_k(U_l U_{0-m-n-k-l} + V_l V_{0-m-n-k-l}) \\ \sum \Gamma_m U_n V_{0-m-n} \\ U_{+1} \\ \vdots \end{Bmatrix} \tag{23}$$

where, for example,

$$\sum \Gamma_m U_n U_{0-m-n}$$

means the sum of all of the terms resulting from the original triple summation that multiply $\exp(j0\omega t)$.

Finally, we note the conservation variables are real quantities, so that

$$U_{-n} = \bar{U}_n \tag{24}$$

where $\bar{U}_n$ is the complex conjugate of U_n. Thus, we only need to store Fourier coefficients for nonnegative n. If N harmonics are retained in the Fourier series representation of the flow, then $2N+1$ coefficients are stored for each flow variable (one for the zeroth harmonic or mean flow and $2N$ for the real and imaginary parts of the remaining harmonics).

The authors originally developed their computional model based on the form of the harmonic balance equations just given. The method produces accurate unsteady flow solutions. However, the computation of the harmonic fluxes is difficult and computationally expensive; on the order of N^3 operations are required, so that the cost of the harmonic balance analysis grows rapidly with the number of harmonics. Also, this approach is not readily applicable to viscous flows because turbulence models tend to be quite complex and not readily expressed in simple algebraic forms.

To alleviate these problems, we note that, alternatively, one can reconstruct the Fourier coefficients of the conservation variables $\tilde{\boldsymbol{U}}$ and the flux vectors $\tilde{\boldsymbol{F}}$ and $\tilde{\boldsymbol{G}}$ from a knowledge of the temporal behavior of $\boldsymbol{U}$, $\boldsymbol{F}$, and $\boldsymbol{G}$ at $2N+1$ equally spaced points over one temporal period. In other words,

$$\tilde{\boldsymbol{U}} = \boldsymbol{E}\boldsymbol{U}^* \tag{25}$$

where $\boldsymbol{U}^*$ is the vector of conservation variables at $2N+1$ equally spaced points in time over one temporal period and $\boldsymbol{E}$ is matrix that is the discrete Fourier transform operator. Conversely,

$$\boldsymbol{U}^* = \boldsymbol{E}^{-1}\tilde{\boldsymbol{U}} \tag{26}$$

where $\boldsymbol{E}^{-1}$ is the corresponding inverse Fourier transform operator. Similar expressions hold for the flux vectors.

Substitution of Eq. (25) into Eq. (21) gives

$$\frac{\partial \boldsymbol{E}\boldsymbol{F}^*}{\partial x} + \frac{\partial \boldsymbol{E}\boldsymbol{G}^*}{\partial y} + j\omega\boldsymbol{N}\boldsymbol{E}\boldsymbol{U}^* = 0 \tag{27}$$

where $\boldsymbol{N}$ is a diagonal matrix with n in the entries corresponding to the nth harmonic. Premultiplying Eq. (27) by $\boldsymbol{E}^{-1}$ gives

$$\frac{\partial \boldsymbol{F}^*}{\partial x} + \frac{\partial \boldsymbol{G}^*}{\partial y} + \boldsymbol{S}^* = 0 \tag{28}$$

where

$$\boldsymbol{S}^* = j\omega\boldsymbol{E}^{-1}\boldsymbol{N}\boldsymbol{E}\boldsymbol{U}^* \approx \frac{\partial \boldsymbol{U}^*}{\partial t} \tag{29}$$

The product $j\omega\boldsymbol{E}^{-1}\boldsymbol{N}\boldsymbol{E}$ is just the spectral operator that approximates $\partial/\partial t$. The advantage of Eq. (28) over the original form of the harmonic balance equations, Eq. (21), is that the fluxes in Eq. (28) are much easier to compute. The fluxes are simply computed at each of the $2N+1$ time levels in the usual way, using Eq. (13). Also, the alternate form of the harmonic balance equations can easily be applied to more complex flow equations, such as the Navier–Stokes equations, whereas the original form, Eq. (21), cannot.

Numerical Solution Technique

To solve the harmonic balance equations, we introduce a pseudotime term so that the equations may be marched to a steady-state condition using a conventional CFD scheme. Using the harmonic balance form of the Euler equations as an example, we let

$$\frac{\partial \boldsymbol{U}^*}{\partial \tau} + \frac{\partial \boldsymbol{F}^*}{\partial x} + \frac{\partial \boldsymbol{G}^*}{\partial y} + \boldsymbol{S}^* = 0 \tag{30}$$

where τ is a fictitious time, used only to march Eq. (30) to steady state, driving the pseudotime term to zero. Note that pseudotime

harmonic balance equations, Eq. (30), are similar in form to the original time-domain form of the Euler equations, Eq. (12).

In Eq. (30), we use a spectral operator to compute the time $\boldsymbol{S}^*$ term, as described in the preceding section. As presented, this operator requires $\mathcal{O}(N^2)$ operations to compute. However, the calculation of the flux vector terms is greatly simplified, requiring only $\mathcal{O}(N)$ computations. As a practical matter, the flux calculations, and other calculations requiring $\mathcal{O}(N)$ computations, require much more computational time than the relatively simple time derivative term. Thus, the computational time scales like the number of Fourier terms retained in the solution.

The method has some similarities to the dual time step method, used by Davis et al.,[18] Sayma et al.,[19] and others to compute unsteady flows in the time domain. Our approach, however, has a number of important differences. First, in the dual time-step method, one marches from one time level to the next time accurately, using pseudotime to drive the residual of the time-accurate equations to zero. The process is repeated over many time steps for several periods T until a periodic solution has been reached. In our approach, we store the solution at just a few points over a single period, and the solutions at all temporal points are advanced simultaneously using pseudotime marching until the solution converges. Second, because we solve for the solution over one complete period, a spectral operator may be used to compute the physical time derivative $\partial/\partial t$ [see Eq. (29)]. The spectral time derivative is much more accurate than finite difference operators, which are used in the dual time-step approach. Therefore, many fewer physical time levels are required using the present method. In fact, in the limit of small-amplitude disturbances, only $2N+1$ time levels per period are required to obtain exact temporal derivatives.

The computational domain may be reduced to a single blade passage, with complex periodicity conditions applied along periodic boundaries. Consider, for example, the density. Spatial periodicity requires that

$$\rho(x, y+G, t) = \rho(x, y, t+\Delta t) \tag{31}$$

Substitution of the boundary condition into the Fourier series for ρ gives

$$\sum_n R_n(x, y+G)\exp(j\omega n t) = \sum_n R_n(x, y)\exp[j\omega n(t+\Delta t)] \tag{32}$$

Dividing Eq. (32) by $\exp(j\omega n t)$, making use of the relation $\Delta t = \sigma/\omega$, and comparing the two series term by term gives the desired periodic boundary conditions

$$R_n(x, y+G) = R_n(x, y)e^{j\sigma n} \tag{33}$$

Similar conditions exist for the remaining conservation variables.

In the present investigation, we solve the Navier–Stokes equivalent to Eq. (30) with modifications required for deforming computational grids. The general numerical solution procedure is as follows. First, $2N+1$ computational grids are generated, one for each time level, using an elliptic grid generator.[20] Here, we use an H–O–H grid topology (Fig. 1). At each node of these $2N+1$ grids, we store the conservation variables $\boldsymbol{U}$. The vector $\boldsymbol{U}^*$ is the vector of these $2N+1$ subvectors.

Next, the pseudotime harmonic balance equations are discretized using standard CFD techniques. In the present investigation, we use a two-step Lax–Wendroff scheme to discretize the harmonic balance equations. The Lax–Wendroff scheme is a node-centered conservative finite volume scheme. A combination of second and fourth differences smoothing is used to capture shocks. Also, because only steady-state solutions are desired, we use local time stepping and multiple-grid acceleration techniques to speed convergence.

At each iteration, boundary conditions must be applied to the solution $\boldsymbol{U}^*$. On the airfoil surface, no-slip and isothermal wall boundary conditions are applied.

To apply the periodicity conditions, the solution $\boldsymbol{U}^*$ along the periodic boundary is Fourier transformed using Eq. (25), and the resulting Fourier coefficients $\tilde{\boldsymbol{U}}$ are modified so that the complex periodicity conditions are satisfied [Eq. (33)]. The resulting modified Fourier coefficients along the computational boundary are then inverse Fourier transformed using Eq. (26), and the results loaded back onto the boundary of the individual grids.

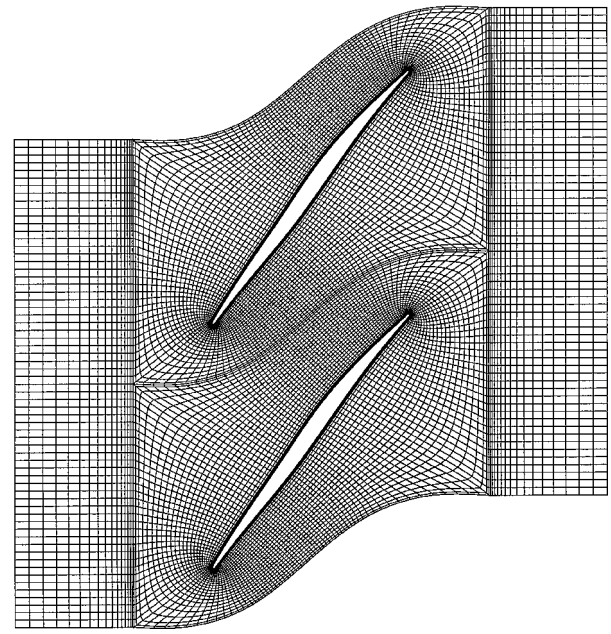

Fig. 1 Computational grid for front stage transonic compressor rotor; two passages are shown for clarity.

The far-field boundary conditions are also applied in the frequency domain because essentially exact nonreflecting far-field boundary conditions are available, greatly improving the accuracy of the method.[21,22] Again, the solution along the upstream and downstream boundaries is Fourier transformed. Conventional steady flow boundary conditions are applied to the mean flow Fourier coefficients ($n=0$). Upstream, we specify total pressure and density and circumferential velocity. Downstream, we specify the static pressure. Nonreflecting boundary conditions are applied to each of the Fourier coefficients with nonzero frequency ($n \neq 0$). Finally, the Fourier coefficients are inverse Fourier transformed, and the results are loaded onto the individual grids. We note that the solutions at the $2N+1$ time levels are only coupled through the spectral time derivative term and the far-field boundary conditions.

The method described in this section is similar to the nonlinear harmonic Euler method described by He and Ning[15] but has two fundamental differences. First, He and Ning use only a single harmonic. Our results demonstrate that solutions computed using a single harmonic may be inaccurate, especially for flows with large shock motions. Second, He and Ning do not make the transformation from the frequency domain to the time domain (the dual time-step approach) described in the preceding section. The dual time step greatly reduces the computational time when multiple harmonics are retained in the model, and greatly simplifies the incorporation of viscous terms and turbulence models when applied to the Navier–Stokes equations.

Computational Results

In this section, we apply the harmonic balance technique to a representative flutter problem. We consider the front stage transonic rotor of a modern high-pressure compressor. Shown in Fig. 1 is a typical computational grid used to compute the two-dimensional flow near the tip of the rotor. At this spanwise station, the inflow Mach number M is 1.27, the inflow angle Θ, measured from the axial direction, is 59.3 deg, and the Reynolds number Re is about 1.35×10^6. The computational grid used is an H–O–H grid, which has good resolution near the airfoil surface for resolving viscous boundary layers, as well as good resolution in the far field for modeling outgoing waves.

Shown in Fig. 2 is the steady flow, that is, no unsteady disturbances, in the blade row computed using a grid with 193×33 nodes in the O-grid section. Note the fairly complex shock structure, with a shock extending from the leading edge both above and below the

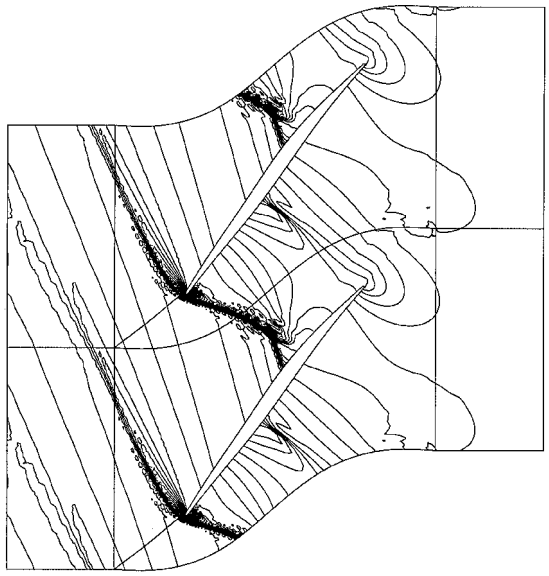

Computed steady pressure

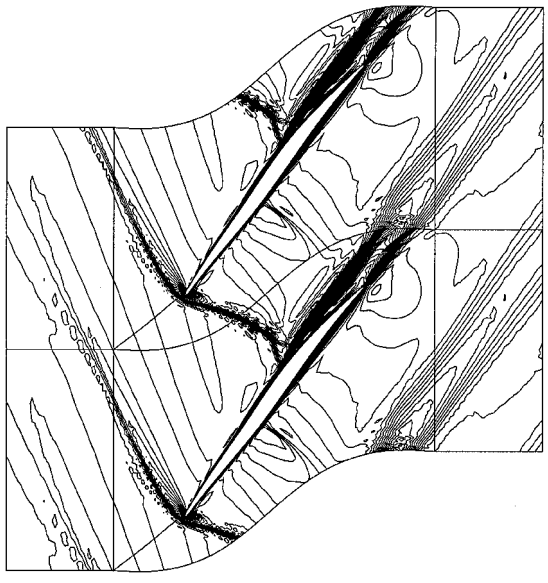

Mach number contours

Fig. 2 Transonic viscous flow through front stage compressor rotor.

airfoil. This shock impinges on the suction surface of the airfoil, causing a local strong adverse pressure gradient, which in turn causes the boundary layer to separate. The rapid growth of the boundary layer results in an oblique shock forming just upstream of the separation point. Also, the flow accelerates over the front portion of the pressure surface, resulting in a weak normal shock at about 40% of the chord on the pressure surface. The pressure distribution on the airfoil surface is shown in Fig. 3, computed using several different grids, with 97×17, 145×25, 193×33, and 241×41 computational nodes in the O-grid region. As the grid resolution increases, the computed shock becomes somewhat sharper. However, away from the shock, all four solutions are virtually identical. In all subsequent computations, the grid with 193×33 nodes in the O-grid region is used.

Next, we consider the unsteady aerodynamic response of the rotor for the case where the airfoils vibrate harmonically in pitch about their midchords with a reduced frequency $\bar{\omega}$ equal to 1.0 (based on chord and upstream velocity), an interblade phase angle σ equal to 30 deg, and amplitude $\bar{\alpha}$. Shown in Fig. 4 is the mean pressure distribution (the zeroth Fourier component) computed for two different pitching amplitudes, $\bar{\alpha} = 0.01$ and 1.0 deg. In each case, the harmonic balance solution was computed using one, three, five, and seven harmonics ($N = 1, 3, 5,$ and 7). Note that, in the small-amplitude case ($\bar{\alpha} = 0.01$ deg), the solutions computed using different numbers of harmonics are nearly identical. In this case, the

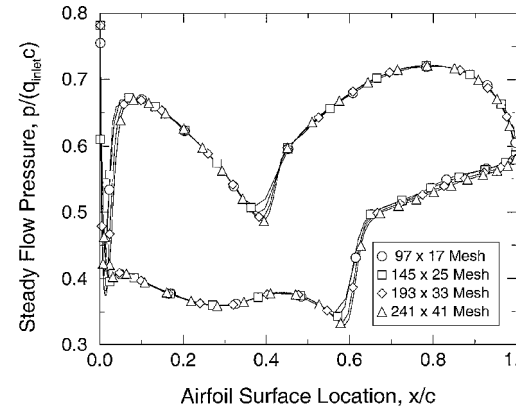

Fig. 3 Steady pressure distribution on surface of front stage compressor rotor airfoils computed using several different grids, with 97 × 17, 145 × 25, 193 × 33, and 241 × 41 computational nodes in the O-grid region of an H–O–H grid.

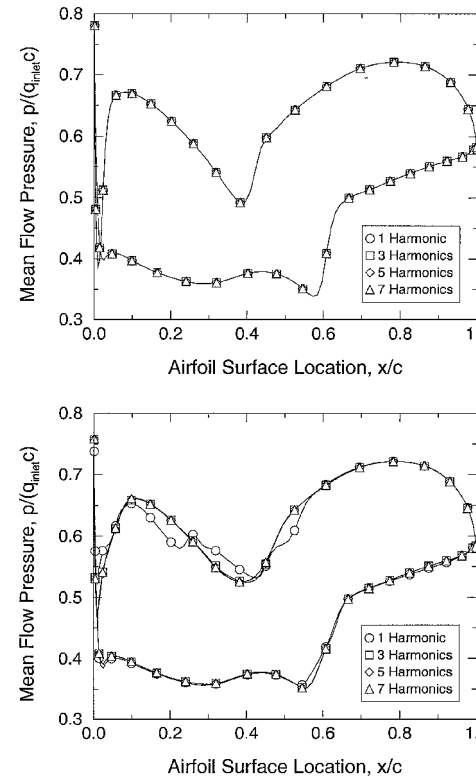

Fig. 4 Zeroth harmonic (mean flow) of unsteady pressure distribution for front stage compressor rotor airfoils vibrating in pitch with $\bar{\omega} = 1.0$ and $\sigma = 30$ deg: top, small-amplitude motion ($\bar{\alpha} = 0.01$ deg); bottom, large-amplitude motion ($\bar{\alpha} = 1.0$ deg).

unsteadiness is so small that nonlinear effects are unimportant and, therefore, the mean flow is unaffected by the unsteadiness. In other words, the mean flow is equal to the steady flow computed with no airfoil motion. For the larger-amplitude motion ($\bar{\alpha} = 1.0$ deg), the mean pressure distributions computed with various numbers of harmonics are now different. However, the solutions converge rapidly as the number of harmonics is increased.

Next, we consider the first harmonic of the unsteady pressure distribution on the airfoil surface. This component is important because it is the only component that contributes to aerodynamic damping for harmonic pitching motion of the airfoil. Shown in Fig. 5 is the first harmonic of the unsteady pressure on the airfoil surface, scaled by the amplitude of the pitching amplitude, again shown for both a small and larger pitch amplitude. As in the case of the mean flow, the computed first harmonic pressure distributions are nearly independent of the number of harmonics retained in the computation. For small-amplitude disturbances, the first and higher harmonics are independent of one another. In fact, the first harmonic solution is the same as one would obtain from a time-linearized solution. For

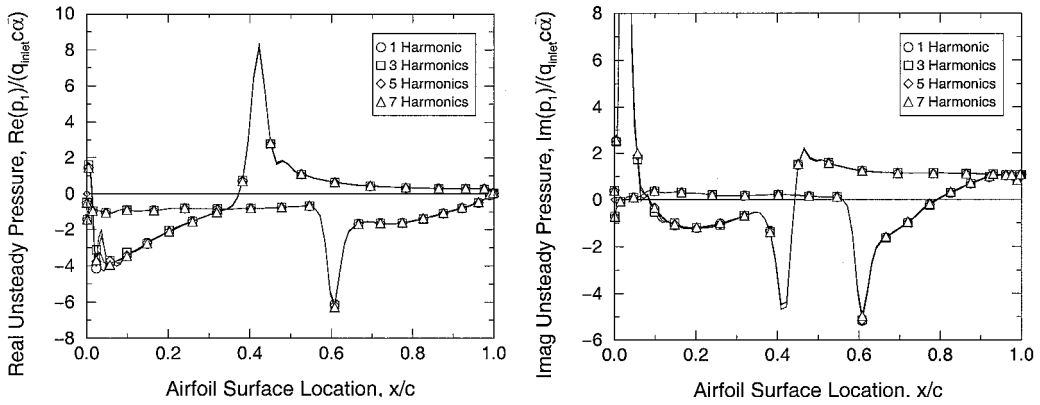

Small-amplitude motion ($\bar{\alpha} = 0.01$ deg)

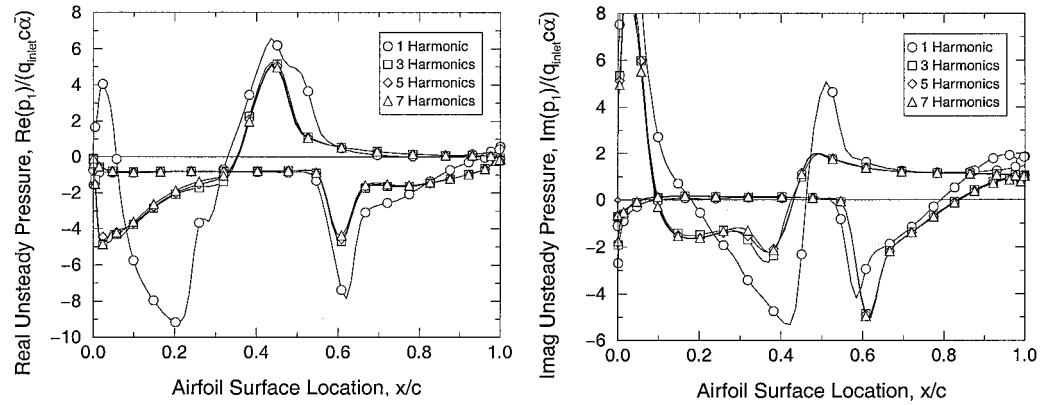

Large-amplitude motion ($\bar{\alpha} = 1.0$ deg)

Fig. 5 First harmonic of unsteady pressure distribution for front stage compressor rotor airfoils vibrating in pitch with $\bar{\omega} = 1.0$ and $\sigma = 30$ deg.

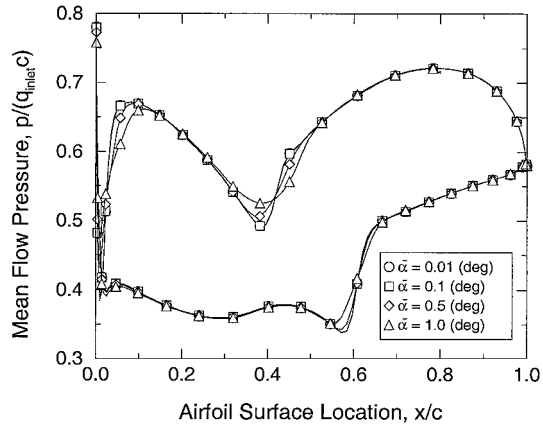

Zeroth harmonic

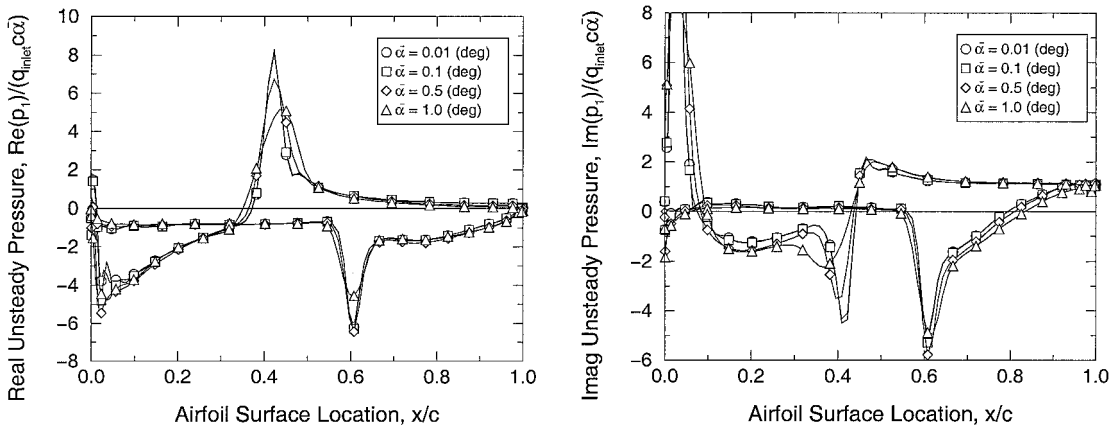

First harmonic

Fig. 6 Unsteady pressure distribution for front stage compressor rotor airfoils vibrating in pitch with $\bar{\omega} = 1.0$ and $\sigma = 30$ deg.

the larger-amplitude pitching motion, on the other hand, the pressure distributions computed with various numbers of harmonics are different, but again the solutions converge rapidly as the number of harmonics is increased.

To demonstrate the influence of nonlinearities on the unsteady flow, we again plot the zeroth and first harmonics of the unsteady flow in Fig. 6. In these results, the larger-amplitude motion solutions are computed using five harmonics so that the results are converged in the harmonic balance sense. The pressure distributions are plotted for several pitching amplitudes. The pressure distributions associated with the larger amplitude pitching motion is seen to be substantially different from the small-amplitude case. In the small-amplitude case, the mean pressure distribution shows signs of very sharp shocks. For the larger-amplitude motion, the shocks get smeared out. Physically, this is because the shocks oscillate, and, when temporally averaged, the shocks appear smeared. Of course, when viewed at any instant in time, the shocks are sharp. Also shown are the real and imaginary parts of the first harmonic of the unsteady pressure. In the small-amplitude case, very large and narrow peaks of pressure are seen. These are the so-called shock impulses associated with the unsteady motion of the shock. As the amplitude of the pitching vibration is increased, these peaks are reduced and spread out, because the shock motion is larger and the resulting shock impulse is spread over a larger chordwise extent.

By appropriate integration of the first harmonic of the unsteady pressure distribution, one can obtain the first harmonic of the pitching moment. The imaginary part determines the aeroelastic stability of the rotor. In the absence of mechanical damping, the rotor is stable only if the imaginary moment is less than zero for all interblade phase angles. Shown in Fig. 7 is the pitching moment as a function of interblade phase angle for several pitching amplitudes. For small-amplitude motions, the rotor is unstable for interblade phase angles σ between -10 and $+60$ deg. Thus, the amplitude of an initially infinitesimal motion will grow. As the motion grows, however, the aerodynamic damping of the least stable interblade phase angle goes to zero. This is seen more clearly in Fig. 8. Shown is the pitching moment for $\sigma = +30$ deg as a function of pitch amplitude computed using one, three, five and seven harmonics. Clearly,

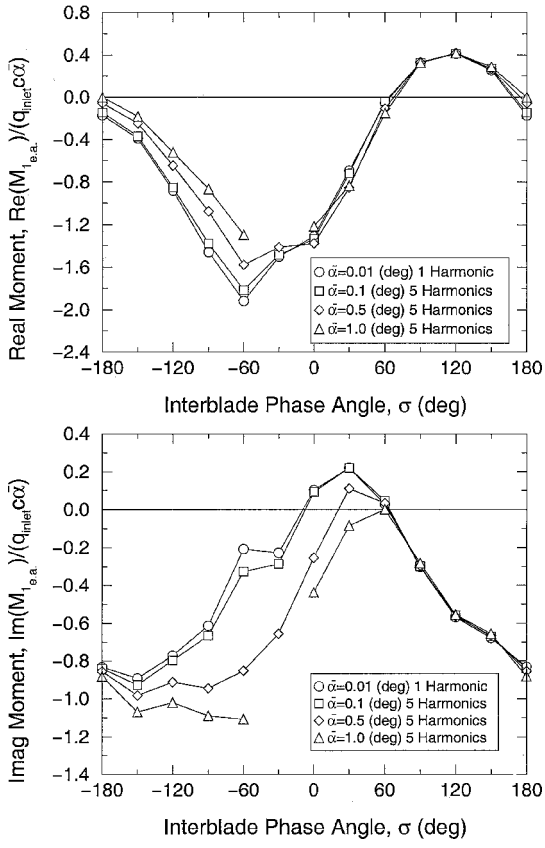

Fig. 7 First harmonic of unsteady pitching moment for front stage compressor rotor airfoils vibrating in pitch with $\bar{\omega} = 1.0$.

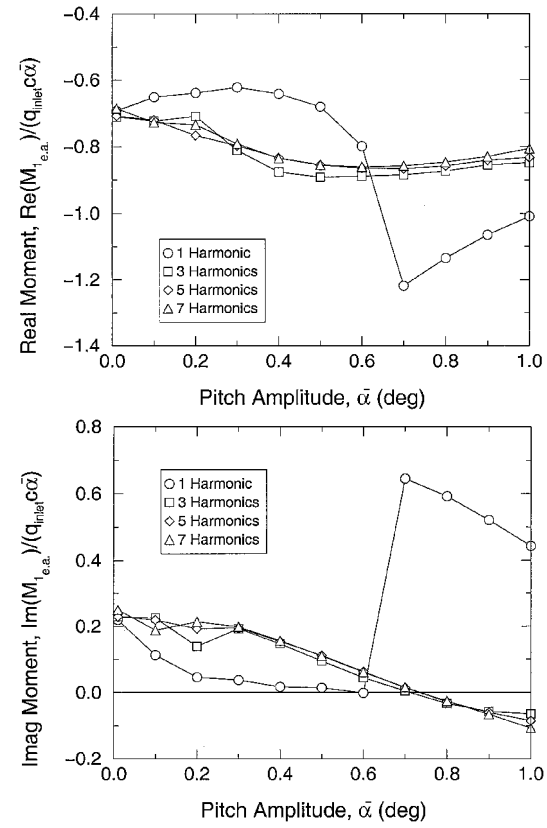

Fig. 8 First harmonic of unsteady pitching moment for front stage compressor rotor airfoils vibrating in pitch with $\sigma = 30$ deg.

the solution computed with just one harmonic is not converged (except at very small amplitudes) and gives erroneous results. However, with three or five harmonics, the solution is converged to engineering accuracy. Note that the imaginary moment is positive (unstable) for small-amplitude motions, but goes to zero at a pitching amplitude of about 0.7 deg. Thus, the blade will vibrate in a stable limit cycle with this pitch amplitude. It is also remarkable that the nonlinear fluid dynamics effects are important at such a small geometric displacement.

We next consider the computational efficiency of the present method. Shown in Fig. 9 are the convergence histories for the steady flow and harmonic balance calculations. Note that, except for $N = 7$, the steady flow solver and harmonic balance flow solver converge in about the same number of iterations. For the $N = 7$ case, the harmonic balance solution does not converge.

The authors believe the nonconvergence is due to an instability pointed out by Giles (personal communication) some years ago when working on time-linearized Euler solvers based on the Lax–Wendroff scheme. A simple Fourier stability analysis reveals that, in principle, such schemes are unconditionally unstable for nonzero frequencies. However, unlike most CFD instabilities, which tend to involve short wavelength disturbances, the instability here is associated with the longest wavelengths. For this reason, a Fourier analysis is not appropriate because it does not include the influence of the far-field boundaries. We have found by analysis and by numerical experiment that the far-field boundaries provide a stabilizing influence. However, if the frequency is too large, as in the case of the higher harmonics, the stabilizing influence of the boundaries is not sufficient to suppress this instability. This is not a serious limitation for two reasons. First, it makes no sense to retain harmonics as high as $N = 7$ because the wavelengths of the disturbances at these high frequencies are too short to be accurately modeled with grid resolutions typically used in unsteady flow calculations. (This limitation also applies to time-domain solution techniques, that is, the high-frequency component of a time-domain solution is unreliable.) Second, we have found that three to five harmonics are more than adequate to obtain mode converged solutions of the zeroth and first harmonic components of the unsteady flow, and the harmonic balance solver usually converges for this number of harmonics.

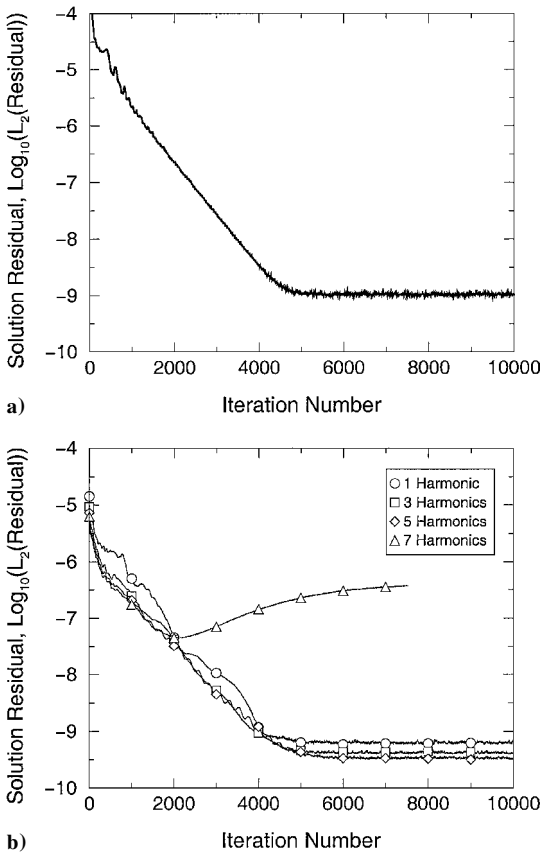

Fig. 9 Convergence history for a) steady flow solver and b) harmonic balance flow solver with $\sigma = 30$ deg, $\bar{\omega} = 1.0$, and $\bar{\alpha} = 1.0$ deg.

Finally, the CPU time per iteration of the harmonic balance flow solver for one, three, five, and seven harmonics was found to be 2.15, 4.62, 7.45, and 10.29 times the cost per iteration of the steady flow solver. Even using seven harmonics, the cost to compute the fully nonlinear, viscous, transonic flow about a vibrating blade row is only about ten times the cost of a comparable steady flow calculation.

Summary

In this paper, a harmonic balance analysis for modeling unsteady nonlinear flows in turbomachinery was presented. The time-domain Euler or Navier–Stokes equations were recast in the frequency domain using harmonic balance concepts. The resulting computational method is computationally efficient, at least one to two orders of magnitude faster than conventional nonlinear time-domain CFD simulations. Furthermore, the method is relatively easy to implement. In this paper, we applied the technique to the two-dimensional Navier–Stokes equations. In unpublished work, we have also applied the technique to the three-dimensional Euler equations.

Computational results demonstrate that even strongly nonlinear flows can be modeled to engineering accuracy with a small number of harmonics and, furthermore, that nonlinear fluid dynamic effects can have a strong influence on the aeroelastic behavior of a blade row. In the example presented in this paper, a transonic front stage rotor of a high-pressure comppressor was found to flutter in torsion, but reaches a stable limited cycle with an amplitude of just 0.7 deg.

Finally, we note that although only applied to the flutter problem in this paper, the method can be used to model a wide variety of important unsteady flow phenomena in turbomachinery. These include the effect of unsteadiness on the time-averaged aerodynamic performance and heat transfer, the aerodynamic forcing resulting from rotor interactions with strong shocks from neighboring blade rows, and rotating stall.

Acknowledgments

This work was funded through a GUIde Consortium on Forced Response of Bladed Disks subcontract from Carnegie Mellon University, Subcontract 537032-57209, with original funding provided through NASA John H. Glenn Research Center at Lewis Field Contract NAS3-27735. Jerry Griffin and Anatole Kurkov are the respective Technical Monitors. This work is part of NASA's Advanced Subsonic Technology program managed by Peter Batterton and John Rhode. Additional support was provided by GE Aircraft Engines.

References

[1]Hodson, H. P., "An Inviscid Blade-to-Blade Prediction of a Wake Generated Unsteady Flow," American Society of Mechanical Engineers, ASME Paper 84-GT-43, June 1984.

[2]Giles, M. B., "Calculation of Unsteady Wake/Rotor Interaction," *Journal of Propulsion and Power*, Vol. 4, No. 4, 1988, pp. 356–362.

[3]Rai, M. M., "Three-Dimensional Navier–Stokes Simulations of Turbine Rotor–Stator Interaction; Part I: Methodology," *Journal of Propulsion and Power*, Vol. 5, No. 3, 1989, pp. 307–311.

[4]Rai, M. M., "Three-Dimensional Navier–Stokes Simulations of Turbine Rotor–Stator Interaction; Part II: Results," *Journal of Propulsion and Power*, Vol. 5, No. 3, 1989, pp. 312–319.

[5]Huff, D. L., Swafford, T. W., and Reddy, T. S. R., "Euler Flow Predictions for an Oscillating Cascade Using a High Resolution Wave-Split Scheme," American Society of Mechanical Engineers, ASME Paper 91-GT-198, June 1991.

[6]He, L., and Denton, J. D., "Three Dimensional Time-Marching Inviscid and Viscous Solutions for Unsteady Flows Around Vibrating Blades," American Society of Mechanical Engineers, ASME Paper 93-GT-92, June 1993.

[7]Whitehead, D. S., and Grant, R. J., "Force and Moment Coefficients of High Deflection Cascades," *Proceedings of the 2nd International Symposium on Aeroelasticity in Turbomachines*, edited by P. Suter, Juris-Verlag, Zurich, 1981, pp. 85–127.

[8]Verdon, J. M., "Linearized Unsteady Aerodynamic Theory," *AGARD Manual on Aeroelasticity in Axial Flow Turbomachines, Vol. 1, Unsteady Turbomachinery Aerodynamics*, edited by M. F. Platzer and F. O. Carta, AG-298, AGARD, 1987, Chap. 2.

[9]Hall, K. C., and Crawley, E. F., "Calculation of Unsteady Flows in Turbomachinery Using the Linearized Euler Equations," *AIAA Journal*, Vol. 27, No. 6, 1989, pp. 777–787.

[10]Hall, K. C., and Clark, W. S., "Linearized Euler Predictions of Unsteady Aerodynamic Loads in Cascades," *AIAA Journal,* Vol. 31, No. 3, 1993, pp. 540–550.

[11]Holmes, D. G., and Chuang, H. A., "2D Linearized Harmonic Euler Flow Analysis for Flutter and Forced Response," *Unsteady Aerodynamics, Aeroacoustics, and Aeroelasticity of Turbomachines and Propellers*, edited by H. M. Atassi, Springer-Verlag, New York, 1993, pp. 213–230.

[12]Hall, K. C., and Lorence, C. B., "Calculation of Three-Dimensional Unsteady Flows in Turbomachinery Using the Linearized Harmonic Euler Equations," *Journal of Turbomachinery,* Vol. 115, No. 4, 1993, pp. 800–809.

[13]Clark, W. S., and Hall, K. C., "A Time-Linearized Navier–Stokes Analysis of Stall Flutter," *Journal of Turbomachinery,* Vol. 122, No. 3, 2000, pp. 467–476.

[14]Giles, M. B., "An Approach for Multi-Stage Calculations Incorporating Unsteadiness," American Society of Mechanical Engineers, ASME Paper 92-GT-282, June 1992.

[15]He, L., and Ning, W., "Efficient Approach for Analysis of Unsteady Viscous Flows in Turbomachines," *AIAA Journal,* Vol. 36, No. 11, 1998, pp. 2005–2012.

[16]Ning, W., and He, L., "Computation of Unsteady Flows Around Oscillating Blades Using Linear and Non-Linear Harmonic Euler Methods," *Journal of Turbomachinery,* Vol. 120, No. 3, 1998, pp. 508–514.

[17]Spalart, P. R., and Allmaras, S. R., "One-Equation Turbulence Model for Aerodynamic Flows," AIAA Paper 92-0439, Jan. 1992.

[18]Davis, R. L., Shang, T., Buteau, J., and Ni, R. H., "Prediction of Three-Dimensional Unsteady Flow in Multistage Turbomachinery Using an Implicit Dual Time-Step Approach," AIAA Paper 96-2565, 1996.

[19]Sayma, A. I., Vahdati, M., Sbardella, L., and Imregun, M., "Modeling of Three-Dimensional Viscous Compressible Turbomachinery Flows Using Unstructured Hybrid Grids," *AIAA Journal*, Vol. 38, No. 6, 2000, pp. 945–954.

[20]Thomas, P. D., and Middlecoff, J. F., "Direct Control of the Grid Distribution in Meshes Generated by Elliptic Equations," *AIAA Journal*, Vol. 18, No. 6, 1980, pp. 652–656.

[21]Giles, M. B., "Nonreflecting Boundary Conditions for Euler Equation Calculations," *AIAA Journal*, Vol. 28, No. 12, 1990, pp. 2050–2058.

[22]Hall, K. C., Lorence, C. B., and Clark, W. S., "Nonreflecting Boundary Conditions for Linearized Aerodynamic Calculations," AIAA Paper 93-0882, Jan. 1993.

A. Plotkin
Associate Editor